Surface-frustrated periodic textures of smectic-*A* liquid crystals on crystalline surfaces

Bruno Zappone[1,*] and Emmanuelle Lacaze[2]

[1]*LICRYL, CNR-INFM Regional Laboratory, and Centro di Eccellenza per i Materiali Innovati Funzionali della Calabria, Università della Calabria, cubo 33b, Rende (CS), 87036 Italy*

[2]*Institut des Nano-Sciences de Paris (INSP), UMR-CNRS 7588, Université Pierre et Marie Curie - Paris 6, 140 rue de Lourmel, 75015 Paris, France*

(Received 28 July 2008; published 10 December 2008)

Using polarizing optical microscopy we studied thin films and droplets of smectic-*A* 4-cyano-4′-n-octylbiphenyl (8CB) liquid crystal deposited in air on crystalline surfaces of muscovite mica that induce monostable planar anchoring. The competition with the homeotropic anchoring at the 8CB-air interface leads to the formation of one-dimensional (1D) patterns composed of straight, parallel defect domains that are organized in periodic arrays over areas as large as several mm^2. We have developed a simple model which identifies the arrays with self-assembled "oily streaks," comprising straight disclination lines and curvature walls. The model reproduces the observed monotonic increase of the period p with the film thickness h in the range $p=1-4$ μm and $h=0.8-17$ μm. For higher values of h we observed a sharp transition to a 2D lattice of fragmented focal conic domains. Despite the apparent generality of our model for hybrid planar-homeotropic anchoring conditions, periodic arrays of straight oily streaks have been observed so far only for 8CB on crystalline surfaces such as mica or MoS_2. Our model indicates that this specificity is due to a particularly strong anchoring of the liquid crystal on such surfaces.

DOI: 10.1103/PhysRevE.78.061704 PACS number(s): 61.30.Hn, 61.30.Pq, 61.30.Jf, 61.30.Eb

I. INTRODUCTION

In recent years, much attention has been devoted to the study of periodic microstructures with strong nonuniformities of their optical properties, for application in photonic band-gap materials [1,2], metamaterials [3], or as templates for guided particle self-assembly [4]. Smectic-*A* (Sm*A*) liquid crystals (LCs) have long been known to form periodic birefringent textures when subject to competing anchoring conditions. *Bidimensional* (2D) lattices have been observed for Sm*A* films deposited in air on isotropic liquids [5,6] or solid surfaces [7,8], or confined between solid plates [9,10]. In each case, the Sm*A* film was subjected to degenerate planar or tilted anchoring at one interface and to homeotropic anchoring at the other interface. An example is given in Fig. 1, where the Sm*A* film rests upon a solid substrate inducing planar anchoring while the anchoring is homeotropic at the Sm*A*-air interface. A uniform texture with all molecules perpendicular to the substrate [homeotropic texture, Fig. 1(a)] or parallel to it (planar texture) involves complete breaking of the anchoring at one of the surfaces [the planar anchoring at the solid substrate in Fig. 1(a)]. Depending on the strength of the anchoring, this process may involve a large surface energy. Both anchoring conditions can be satisfied by introducing a defect domain of the type described in Fig. 1(b), which can lower the surface energy to the expenses of volume energy in a region of lateral extension $2r$. On surfaces inducing a degenerate (rotationally invariant) planar anchoring, defect domains are or include part of a toroidal focal conic domain (FCD) [Fig. 1(c)], where the conjugated ellipse and hyperbola become, respectively, a circle of radius r anchored at the surface and a straight vertical line, t [11]. Toroidal FCDs self-assemble into close-packed lattices that minimize the area of the substrate between neighboring FCDs, where the orientation of molecules violates the planar anchoring conditions [12].

For anisotropic surfaces that align the Sm*A* molecules along a well-defined direction (nondegenerate, monostable planar anchoring), the geometry of the defect is expected to be *monodimensional* (1D) and invariant for translations perpendicular to the planar anchoring direction (easy axis). Starting from the domain structure of Fig. 1(b), curved smectic layers form concentric cylinders wrapped around straight disclination lines c. The line t degenerates into a vertical "curvature wall" [or "tilt grain boundary," Fig. 1(d)] [13] at distance r from both disclinations. This type of defect domain, known as an oily streak (OS), is common for Sm*A* samples confined under homeotropic anchoring conditions [14–16], possibly subjected to external electric fields [17] or shear [18]. Although the straight OS domain structure may appear typical of hybrid planar-homeotropic anchoring conditions [Fig. 1(d)], it has been observed so far for one particular system: films of 4-cyano-4′-n-octylbiphenyl (8CB) deposited in air on crystalline surfaces of molybdenite (MoS_2) [13].

In this work we show that OS domains can also be obtained for 8CB deposited on muscovite mica, which is also a crystal. As for toroidal FCDs, OSs also self-assemble into periodic arrays that are remarkably straight and well aligned with respect to the anchoring direction of mica [Fig. 1(d)]. We measured the period of the arrays as a function of the optical phase retardation at the curvature walls, which is related to the thickness, and compared the results to the relation expected on the basis of the elastic theory of smectics. We found that experiments and theory agree well if we consider a very high strength of the planar anchoring, which is probably shared among crystalline surfaces such as mica and MoS_2. We also observed a sharp thickness-induced transition

*Corresponding author. zappone@fis.unical.it

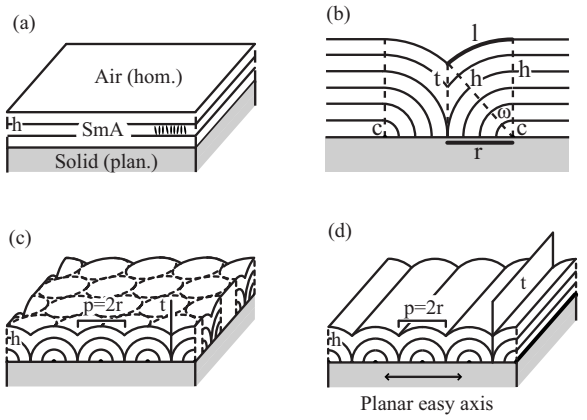

FIG. 1. Structures of a Sm*A* film of thickness h confined between a flat solid surface inducing planar anchoring and the free interface with air, inducing homeotropic anchoring. (a) Uniform homeotropic configuration. The average orientation of the Sm*A* molecules is perpendicular to the planes shown in the figure. (b) Cross section of an isolated defect domain with half-width r. The domain is symmetric around the vertical line t. Points c are centers of curvature for the smectic layers. The free interface is bent over a length $2l$ and its normal deviates from the vertical by a maximum angle ω such that $r=h\sin\omega$ and $l=h\omega$. (c) A toroidal focal conic domain can be created on planar degenerate surfaces by rotating (b) around the line t, which becomes a singular line. Rotation of points c creates a circular defect loop. Toroidal FCD self-assemble in a hexagonal lattice of period $p=2r$. (d) An array of cylindrical defect domains or oily streaks (OSs) can appear on crystalline surfaces inducing nondegenerate planar anchoring. Each domain is created by uniformly translating (b) in a direction perpendicular to the planar easy axis and to the line t, which becomes a curvature wall. Points c become straight disclination lines.

to a 2D lattice of nontoroidal, fragmented FCD of the type recently discussed by Lavrentovich and Kleman [19]. The possibility of creating 1D and 2D periodic patterns of birefringent Sm*A* covering areas of the mica surface as large as several mm^2 appears interesting for studying defect structure, nucleation, and self-assembly in structured materials as well as for possible applications in photonics.

II. MATERIALS AND METHODS

Mica is a layered alumino-silicate crystal that can be cleaved in large, transparent, and atomically smooth sheets exposing a same crystallographic plane over an area up to 1 cm^2. In our experiments, droplets of Sm*A* 8CB (from Merck, Germany) of volume less than 0.1 μl were deposited on freshly cleaved plates of muscovite mica (from S&J Trading, USA) of thickness 0.1–0.3 mm. After a few minutes, the sample was heated to the nematic phase and the droplet started spreading on the surface. The spreading continued for a few hours until the thickness at the edge of the droplet reduced to a few micrometers. The sample was then brought back to the Sm*A* phase and imaged at room temperature with a polarizing optical microscope in transmission. We noticed that the planar anchoring of nematic 8CB on mica deteriorated to homeotropic within a few hours in the presence of humidity higher than about 30% [20]. To avoid this, we let the droplet spread in an enclosure containing water-adsorbing silica gel. Spreading of the droplet and deterioration of the anchoring were much slower (typically 24 h) in the Sm*A* phase.

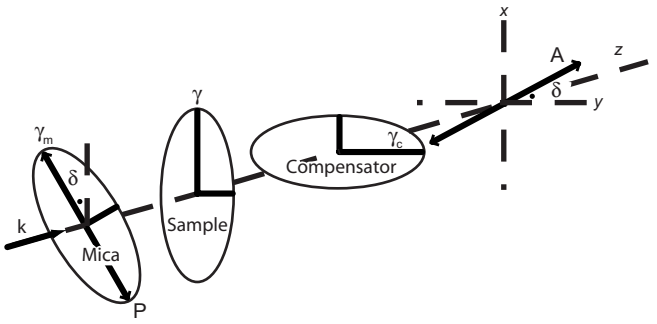

FIG. 2. Setup used to measure the difference in optical path between ordinary and extraordinary polarizations of 8CB films on mica using an optical compensator. Light propagates along the z direction with wave vector $k=2\pi/\lambda$. The x axis is parallel to the planar easy axis γ. The polarizer P is parallel to the slow optical axis of mica, γ_m, which forms an angle δ with γ. The slow axis γ_c of the compensator is at 90° with γ. The analyzer A is crossed at 90° with P.

We measured the phase retardation of the 8CB at different locations of the droplet using a Berek-type tilting compensator (from Leitz, Germany) with a compensation range of $5\lambda\approx 2.75$ μm. Since the birefringence of the 8CB is $\delta n_{\max}=0.14$ [21], the compensator was able to compensate the full (planar) birefringence of a film of thickness up to $h<5\lambda/\delta n_{\max}\approx 19.6$ μm. Mica plates are birefringent ($\delta n_{\text{mica}}\sim 0.005$) under normal incidence of light. Liquid crystals compounds of the nCB series generally become anchored on mica along a direction γ oblique to the mica slow axis γ_m [20]. Under conflicting planar and homeotropic anchoring conditions, the molecular director is expected to adopt a splay-bend configuration (without twist). The distorted director lies in a plane parallel to γ, normal to the mica substrate and, in the Sm*A* phase, perpendicular to the OSs. A monochromatic wave with wave vector k traveling through the 8CB film at a location x on the substrate where the thickness is l experiences a phase retardation between the extraordinary polarization (parallel to the splay-bend plane) and the ordinary polarization (normal to the plane). The difference in optical path between the two polarizations is given by

$$\varphi(x)=\int_0^{l(x)}\frac{n_e n_o}{\sqrt{n_o^2\cos^2\psi(x,z)+n_e^2\sin^2\psi(x,z)}}dz-n_o l(x)$$
$$=\delta n(x)l(x), \qquad (1)$$

where ψ is the tilt angle of the director at a point (x,z) of the splay-bend plane, n_e and n_o are respectively the extraordinary and ordinary refractive indices of 8CB, and $\delta n(x)$ is the local birefringence.

To measure φ, we aligned the polarizer with the mica axis γ_m and the slow optical axis of the compensator with the planar easy axis γ of 8CB on mica (Fig. 2). The analyzer was crossed at 90° with the polarizer. The light intensity trans-

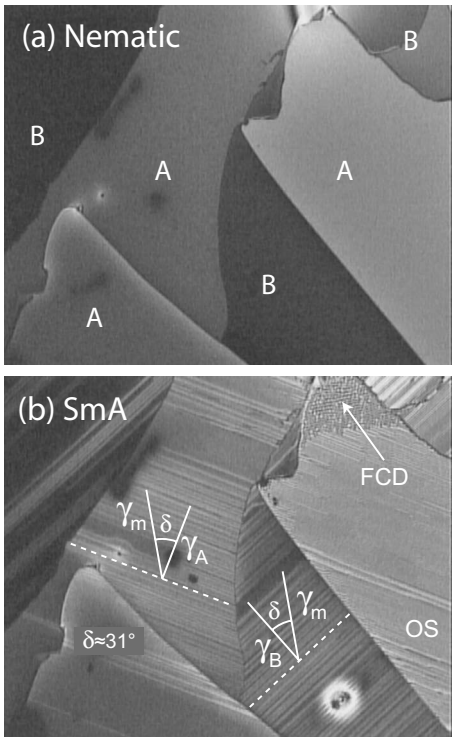

FIG. 3. Thin film of 8CB at the edge of a droplet deposited in air on mica. The slow optical axis, γ_m, of mica is parallel to the polarizer, so that bare mica appears dark (not shown), while regions coated by 8CB appear colored. (a) Nematic phase. Sharp-edged patches labeled *A* or *B* are domains of uniform anchoring of the LC and correspond to the two types of lattices present on the surface of a cleaved mica sheet. (b) Smectic phase. OSs appear as linear strips in the bright patches, oriented along the two directions indicated by the dotted lines. The two directions of planar anchoring, γ_A and γ_B, that correspond to the two surface lattices of the mica, are perpendicular to the OS [see also Fig. 1(d)] and form the same angle $\delta \approx 31°$ with the mica optical axis, γ_m. Notice the FCD in the thicker region of the film marked by an arrow.

mitted through the analyzer was proportional to $\sin^2[k(\varphi - \varphi_c)/2]$ where φ and φ_c are the path differences respectively inside the sample [Eq. (1)] and the compensator. Total extinction was therefore obtained for $\varphi = \varphi_c$, where φ_c could be read from the compensator. In our experiments, we measured φ in regions of maximum birefringence of the OSs, where curvature walls are expected [Fig. 1(b)]. In Sec. IV, we will show that there is a one-to-one correspondence between the path difference φ at the location of a curvature wall and the thickness h of the 8CB film [Fig. 1(b)]. We used the theoretical $\varphi(h)$ curve as a conversion chart to indirectly determine h as a function of the values of φ measured in the Sm*A* phase.

We measured the lateral size of the OS, $2r$ [Fig. 1(d)], from digitized micrographs of the 8CB droplets.

III. EXPERIMENTAL RESULTS

Figure 3(a) shows a film of nematic 8CB spreading on a mica plate. The plate was oriented with its slow optical γ_m parallel to the polarizer (Fig. 2) and appeared completely dark (without compensator) before being coated by 8CB. Colored patches in Fig. 3(a) indicate regions where the orientation of the 8CB director, averaged over the film thickness, was oblique to both γ_m and the normal to the plate. 8CB [22] and other LCs of the cyanobiphenyl (*n*CB) family adopt a planar anchoring on mica, while the anchoring is homeotropic at the interface with air [20]. Therefore, in the nematic phase the director of the 8CB was expected to continuously rotate by 90° going from mica to the free interface with air (splay-bend distortion [11]). This configuration typically shows much larger spatial-temporal fluctuations of the local birefringence than uniform planar or homeotropic textures. This effect was observed in our experiments, confirming the hybrid nature of the anchoring conditions and the tilted average orientation of the molecules in nematic films. Patches of nematic 8CB on mica were uniformly colored [bright and dark tones *A* and *B* in Fig. 3(a)] and had sharp edges corresponding to nanoscopic crystallographic steps left on the mica surface during cleavage. These steps randomly connect two types of cleavage planes, where atoms are arranged in two different surface lattices related to each other by a 60° rotation [20]. Across a step, the variation of birefringence due to changes of the mica thickness is negligible and the variation of 8CB film thickness is too small and smooth to explain the observed sharp switching between colors [Fig. 3(a)]. The latter is therefore due to an abrupt change of anchoring direction across steps connecting different surface lattices with two possible easy axes, γ_A and γ_B. We point out that in each cleavage domain of the mica surface the planar anchoring direction is unique (monostable anchoring along γ_A or γ_B). In contrast, 8CB on MoS_2 can adopt multiple anchoring orientations (multistable anchoring) on a same cleavage plane [23].

After cooling down the sample to the Sm*A* phase, regular arrays of OSs appeared [Fig. 3(b)] for thin 8CB films. The arrays were oriented along two well-defined directions. Since the cylindrical axis of a linear defect is expected to be perpendicular to the local easy axis [Figs. 1(b) and 1(d)], γ_A or γ_B, the orientation of the array immediately reveals the orientation of this axis [Fig. 3(b)]. We found that γ_A and γ_B are symmetrical with respect to the mica optical axis γ_m at the same angle of $\delta \approx 31°$. This behavior is similar to the anchoring of 5CB on mica [20].

The size r of an OS [Fig. 1(d)] increased as we moved from the thin edge to the thicker center of the 8CB droplet [Figs. 4(a) and 4(b)]. The increase was monotonic and continuous along the easy axis, while a stepwise increase was observed along the cylindrical axis of OS (normal to the easy axis) where two or more OSs suddenly merged into a defect with larger radius [dotted ellipses in Figs. 4(a) and 4(b)]. In uniform regions of small thickness, close to the droplet edge, OSs showed the same radius and formed periodic arrays with a well-defined period p. For larger thicknesses closer to the droplet center, r was slightly polydispersed and p was less defined.

Figure 5 is an example of optical compensation of an array of OSs obtained using the tilting compensator. The slow optical axis of the underlying mica plate was parallel to the polarizer (Fig. 2), so that bare (uncoated) mica appeared dark. Without compensator [Fig. 5(a)], the texture appeared

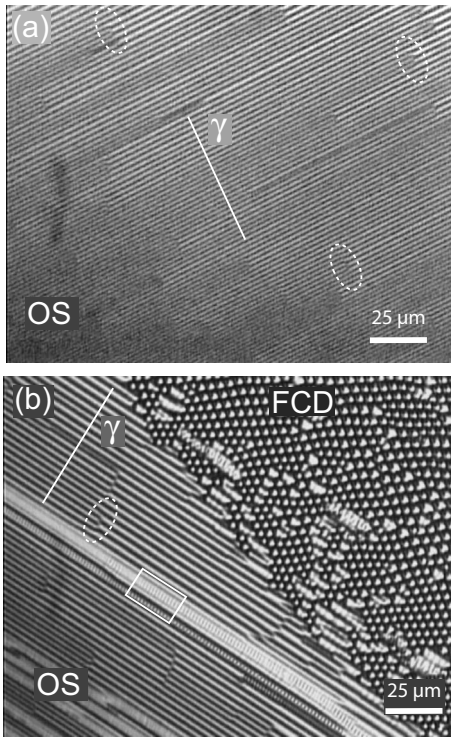

FIG. 4. Textures of Sm*A* 8CB deposited on mica in air and observed between crossed polarizers (no compensator). In (a) and (b), the mica optical axis was aligned with the polarizer. The gradient of thickness was approximately directed from the lower left to the upper right corner. γ is the direction of planar anchoring. (a) Periodic arrays of OSs observed for thin films. Ellipses mark the points where two or more defects merge in a larger defect. (b) A thicker region of the 8CB droplet, showing a thickness-induced transition from a 1D array of OS to a domain containing a 2D lattice of FCDs. The rectangle marks isolate OSs with transverse striation, which were equally found in both regions above a certain thickness.

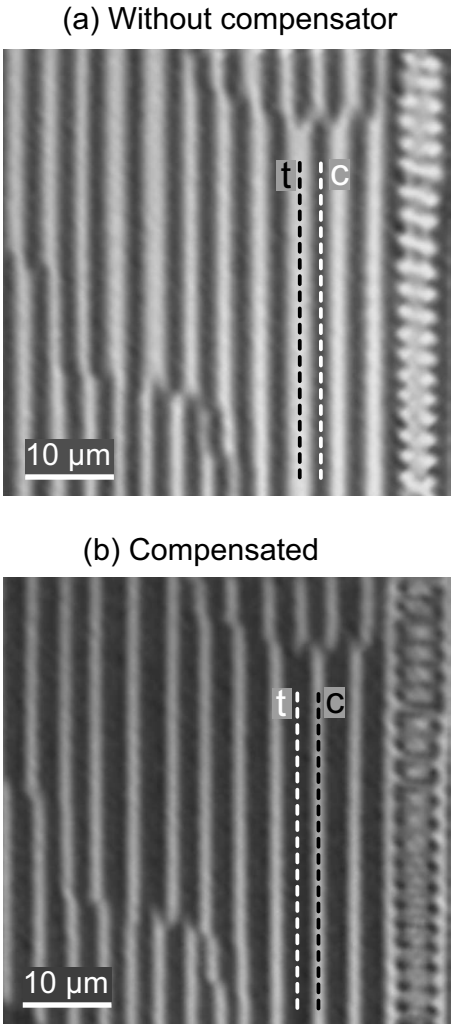

FIG. 5. Array of OSs in the thickest region of the 8CB droplet, immediately before the transition to a 2D lattice of FCDs. Images were taken between crossed polarizers (see Fig. 2 for the alignment of the optical elements). (a) Without compensator, the singular lines *c* of Figs. 1(b) and 1(d) appear dark, while curvature walls *t* appear bright. (b) The same region of the sample after compensating the bright *t* lines with an optical path difference $\varphi \approx 205$ nm. Notice the dispersion of defect sizes and the presence of domains (to the right of the images) with a transverse periodic striation.

as a series of alternating bright and dark parallel bands. Dark bands corresponded to an average homeotropic alignment of the director, which we identify with the region of the OS containing the disclination [lines *c* in Fig. 1(b)], while bright bands correspond to the curvature wall [*t* in Figs. 1(b) and 1(d)]. The distance between two consecutive dark and bright bands is the radius *r* of the defect [distance *c*-*t* in Fig. 1(b)]. The period of the array was calculated as $p=2r$, averaging *r* over at least five bright bands. We compensated the optical phase retardation at the centerline of bright bands [Figs. 5(a) and 5(b)]. A curve showing the period *p* of the linear arrays as a function of the optical path difference φ is given in Fig. 6. The period could be resolved by optical microscopy down to a minimum value of about 0.5 μm. For smaller thicknesses close to the edge of the droplet, the OS array continued into a birefringent (nonhomeotropic) texture, where OS domains, if present, could not be resolved.

As the thickness of the 8CB film increased going from the edge to the center of the droplet, we observed a sharp transition from OSs to FCDs (Fig. 7) at a well-defined thickness. FCDs were self-organized in a 2D lattice that was almost hexagonal, with a lattice distance of about 4 μm for thickness close to the transition to OSs. One of the lattice vectors [α in Figs. 7(a) and 7(b)] was approximately parallel to the easy axis γ and perpendicular to the linear defects. The unit cell of the FCD lattice showed a fan-shaped anisotropic texture aligned with γ and spanning an angle $\tau \approx 75°$ [Fig. 7(c)]. We interpret these structures as fragmented FCDs having incomplete ellipses anchored at mica surface [14,19]. The conjugated hyperbolas cross the plane of the substrate at the vertices of the fan textures and their asymptotes point outward from the 8CB/air interface. Interestingly, the oriented fan-shaped FCDs never pointed at each other with their vertices, despite the symmetry of the planar anchoring conditions for rotations of 180° around the substrate normal. Close to the transition between the 1D array of OSs and the 2D lattice of FCDs, the size of a fan texture measured along γ was close to the size, $2r$, of an OS. The size of the fan texture

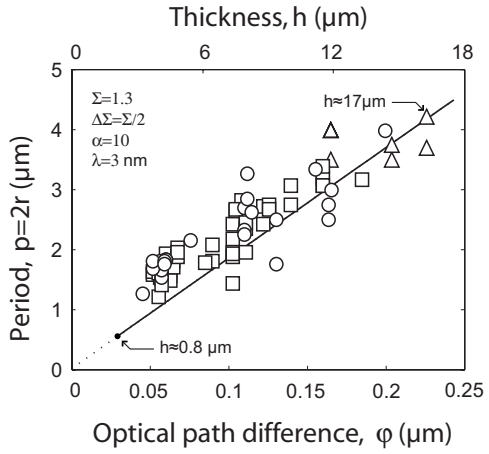

FIG. 6. Period p of an array of OSs as a function of the optical path difference φ measured with a compensator at the location of the curvature wall [Fig. 1(d)]. Circles, squares, and triangles represent data from three different 8CB droplets on mica at temperatures of 26–29 °C. Periods smaller than $p=0.5-0.6$ μm were not resolved by optical microscopy. For $\varphi>0.23$ μm, the array transformed into a 2D lattice of FCDs. The solid line is a theoretical curve calculated from Eqs. (1) and (11). The model parameter Σ, λ, $n_e=1.66$, and $n_o=1.52$ [21] were taken from the literature, whereas $\alpha=10$ and $\Delta\Sigma=\Sigma/2$ were chosen so as to give a critical period p_0 close to the minimum measured value (black dot). The top axis and arrows show the values of the film thickness h calculated from the measured values of φ (see Sec. IV B)

and the lattice period increased with the thickness h, while the fan aperture angle τ was constant. The increase of size was accompanied by an increased polydispersity similar to that observed for OSs. We could not determine the exact geometry of the FCD, which prevented us from extracting a quantitative measurement of h from the phase retardation measured with the compensator.

In both 1D arrays and 2D lattices, we observed isolated streaks with a periodic transverse striation, i.e., a modulation

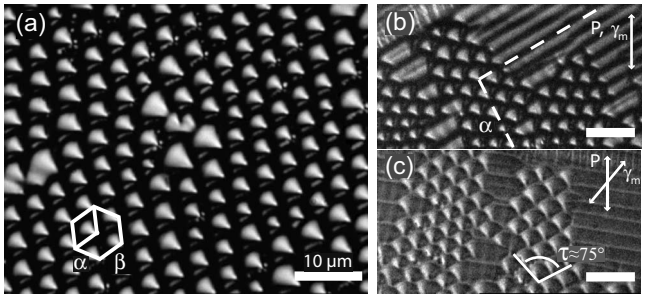

FIG. 7. Bidimensional lattice of FCD of a 8CB droplet on mica. (a) A thick region of the droplet viewed between crossed polarizers (no compensator). FCDs are shaped like fans pointing toward the direction of the lattice vector α. The vector β forms an angle $\approx 120°$ with α. (b) Transition region between the 2D lattice and the 1D array of OSs. The vector α forms an angle $\approx 90°$ with the cylinder axis (dashed line) and it is almost parallel to the planar easy axis. P and γ_m respectively represent the orientation of the polarizer and of the mica optical axis. (c) The same region after rotating the sample between crossed polarizers, highlighting the fan shape of the FCD texture with aperture $\tau \approx 75°$.

of the birefringence along the main axis of the streak. Examples are given in Figs. 4(b) and 5. The period of the striation was smaller that the size r of the domain. Striated domains were parallel to (nonstriated) OSs and completely disappeared at small thickness, leaving only OSs.

IV. MODEL FOR LINEAR ARRAYS

A. Isolated oily streak

We propose a simple model to describe the periodic arrays of linear defects observed for SmA 8CB on mica. First, consider an isolated OS domain [Fig. 1(b)] with radius r, surrounded by a uniform SmA texture. The energy per unit length of the OS differs from the uniform configuration by an amount

$$\Delta F = F_v + 2(l-r)\sigma - 2r\Delta\sigma. \tag{2}$$

The first term, $F_v>0$, describes the increase of energy due to curvature, dilation, and compression of the layered smectic structure in the volume of the film. F_v also includes the energy of the disclination lines c and of the curvature wall t at the center of the OS [Fig. 1(b)]. The second term of Eq. (2), $2\sigma(l-r)>0$, where σ is the surface energy of the smectic-air interface, is the energy required to bend this interface in a cylindrical shape of length $2l$ [Fig. 1(b)]. The last term of Eq. (2), $-2\Delta\sigma r$, contains the difference in surface energy $\Delta\sigma=\sigma_h-\sigma_p$ between a homeotropic alignment (σ_h) and a planar alignment (σ_p) of the director at the SmA-mica interface. Since $\Delta\sigma>0$ for planar anchoring, the last term of Eq. (2) is negative. To create a stable defect ($\Delta F<0$), this last term must balance the sum of the positive terms of (2) and *a fortiori* balance the second term, which leads to the condition $(l-r)/r<\Delta\sigma/\sigma$. Since in most situations $\Delta\sigma/\sigma<1$, we consider the case where $0<(l-r)/r\ll 1$. In the construction of Fig. 1(b), where $r=h\sin\omega$ and $l=h\omega$, this case corresponds to $(l-r)/r\approx\omega^3/6\ll 1$, which we will call the small-angle approximation in the following. The opposite situation, where $\omega\approx\pi/2$, corresponds to the disappearance of the curvature wall.

The volume term of Eq. (2) is the sum of four contributions:

$$F_v = F_{\text{inner}} + F_{\text{outer}} + F_{\text{wall}} + F_{\text{core}}. \tag{3}$$

F_{inner} is due to cylindrical smectic layers with radius of curvature smaller than or equal to r [Fig. 1(b)]. F_{outer} is due to layers with radius of curvature between r and h. These terms can be written as

$$F_{\text{inner}} = \frac{\pi}{2}K\ln(r/r_c) \approx \frac{\pi}{2}K\ln(h\omega/r_c),$$

$$F_{\text{outer}} = K\int_{r/h}^{1}\frac{\arcsin t}{t}dt \approx Ka - K\omega, \tag{4}$$

where $K=7\times10^{-11}$ J/m is the curvature elastic constant of 8CB [24] and r_c is the radius of the disclination core. The rightmost side of Eq. (4) is valid only in the small-angle approximation, $r/h\approx\omega\ll 1$. The integral has been developed

to the first order of ω and the adimensional constant $a=1.09$ is its value for $\omega=0$. To derive Eq. (4) we have supposed that the thickness of a smectic layer is constant throughout an OS, so that we only considered the bending elastic energy. In fact, layers dilation becomes significant close to the curvature wall, in a region of width comparable to the smectic penetration length [9], $\lambda=(K/B)^{1/2}\approx 3$ nm, where B is the compression modulus of 8CB [25]. We treat this region as a wall defect in the continuous structure of the OS. Its energy, including bending and dilation of the layers, is given by the third term of Eq. (3):

$$F_{\text{wall}} \approx bK\frac{r}{\lambda} \approx bK\omega\frac{h}{\lambda}. \tag{5}$$

Equation (5) can be derived from the energy of a tilt grain boundary of arbitrary angle [9,13], giving a value of the constant b close to unity [14,19].

The fourth term $F_{\text{core}}\approx cK$ is the energy per unit length (or line tension) of a straight disclination core. We introduce the adimensional variables $f=\Delta F/K$, $x=h/\lambda$, $\Delta\Sigma=\Delta\sigma\lambda/K$, and $\Sigma=\sigma\lambda/K=1.3$, where we have used the value $\sigma=30$ mJ/m^2 for 8CB [13]. Equation (2) becomes

$$f=\alpha-(2\beta x+1)\omega+\Sigma x\omega^3/3, \tag{6}$$

where

$$\alpha=a+c+\frac{\pi}{2}\ln(r/r_c),$$

$$\beta=\Delta\Sigma-b/2. \tag{7}$$

Because of the logarithmic dependence, the quantity α slowly varies with the radius, $r=0.5-2$ μm, measured in our experiments and can be approximated to a constant [6]. We will consider $\alpha\approx 10$ for small values of the core energy $F_{\text{core}}/K=c\approx 1$ and radius $r_c\approx\lambda$ [6,17,26], and $\alpha\approx 50$ for larger core energies $F_{\text{core}}/K=10-100$ [9,27], and radius $r_c\approx 100$ nm, recently found for 8CB on MoS_2 [27].

For a given thickness x a stable defect can be created if the function f of Eq. (7) has a negative minimum for some value of ω. This requires β to be positive [28] in the second term of Eq. (7), i.e., $\Delta\sigma>(b/2)K/\lambda\approx 15$ mJ/m^2. This value is high compared to the typical strength $\Delta\sigma<1$ mJ/m^2 of a planar anchoring in the nematic phase [20].

The limit of stability for a single OS is described by the condition $f(x,\omega)=0$, which defines a single-valued function $x(\omega)$ [solid line in Fig. 8(a)] with an absolute minimum x_0 at an angle ω_0 given by the following relations:

$$\omega_0^2\approx 2\frac{\beta}{\Sigma},$$

$$x_0\approx\frac{h_0}{\lambda}\approx\frac{3}{2}\frac{\alpha}{\Sigma\omega_0^3}. \tag{8}$$

Therefore, stable defects can only be created above a *critical* thickness h_0. For $h<h_0$, the texture of the SmA is uniformly homeotropic. At $h=h_0$, defects are created with a finite radius $r_0\approx h_0\omega_0$. For $h>h_0$, the equilibrium value of Ω as a function of the thickness h can be calculated from the condition $\partial f/\partial\omega=0$:

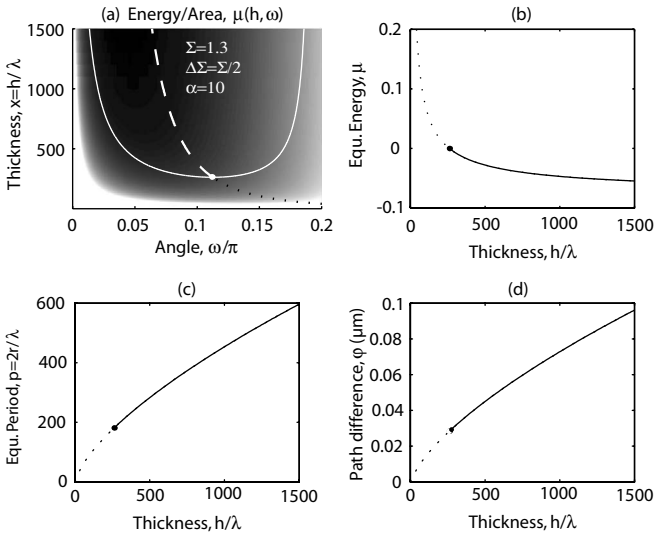

FIG. 8. Periodic array of OS. (a) Energy per unit area, μ, as a function of the angle ω and the film thickness $x=h/\lambda$, normalized by the smectic penetration length $\lambda\approx 3$ nm. μ is calculated from Eq. (10) with $\Delta\Sigma=\Sigma/2$, Σ taken from the literature and $\alpha=10$. The white solid line corresponds to $\mu(x,\omega)=0$. The white dot is the critical point ($x_0=h_0/\lambda=270$, $\omega_0=0.11\pi$) where the function $x(\omega)$ has an absolute minimum. Defects are stable (equilibrium) along the white dashed line for $x>x_0$. The black dotted line for $x<x_0$ indicates metastable states (positive minima of μ). (b) Equilibrium surface energy μ as a function of the thickness h. Black dots and dotted lines indicate respectively critical and metastable points. (c) Equilibrium period, $p/\lambda=2r/\lambda$, normalized by the smectic penetration length λ as a function of h. (d) Equilibrium optical path difference φ as a function of h.

$$\Omega=\sqrt{\frac{2\beta}{\Sigma}+\frac{\lambda}{\Sigma h}}. \tag{9}$$

Therefore, Ω monotonically decreases with h whereas the equilibrium radius $R\approx h\Omega$ monotonically increases.

B. Periodic array of oily streaks

Above the critical thickness, multiple OSs can lower the total energy by reducing their mutual distance so as to maximize the area where the anchoring is planar. Each OS is therefore expected to be in contact with two others, sharing the disclination lines [Fig. 1(d)]. This arrangement produces the periodic arrays of parallel OSs observed experimentally (Fig. 4). For a fixed thickness h we call f the energy of a single streak of lateral extension $2r$ [Fig. 1(b)] and N the total number of OSs in an array. As pointed out by Blanc and Kléman [12], minimizing the total energy Nf of the array for a fixed thickness h amounts to minimizing the energy per unit area μ of the array with respect to ω:

$$\mu=\frac{f}{2r}\approx\frac{K}{\lambda}\left(\frac{\alpha}{2x\omega}-\frac{1}{2x}-\beta+\Sigma\frac{\omega^2}{6}\right). \tag{10}$$

This energy is negative in the same region of the (x,ω) space where $f<0$ [Eq. (6)] and therefore the critical values h_0 and ω_0 for the creation of a periodic array are the same as for an isolated OS [Eq. (8)]. The $\Omega(x)$ curve can be calculated from the condition $\partial\mu/\partial\omega=0$:

$$\Omega = \sqrt[3]{\frac{3}{2}\frac{\alpha\lambda}{\Sigma h}}. \tag{11}$$

As for single defects, Ω decreases with h, while the equilibrium period $P=2R=2h\Omega$ increases as $h^{2/3}$. We notice that Ω depends on the properties of the smectic compound through σ and α but not on the difference of surface energies $\Delta\sigma$. Therefore, different substrates should produce the same $\Omega(x)$ curve. On the other hand, $\Delta\sigma$ determines the critical thickness [via β in Eq. (8)] for which OSs become energetically favorable compared to the homeotropic texture.

Figure 8(a) shows the surface energy μ as a function of $x=h/\lambda$ and ω, as well as the equilibrium $\Omega(x)$ curve for values of Σ taken from the literature on 8CB [29,30] and for small values of the core energy ($\alpha\approx 10$). With the choice of $\Delta\sigma=\sigma/2$, the critical thickness for the appearance of a stable array is $h_0\approx 270\lambda$, while the critical angle is $\omega_0=0.11\pi$, which satisfies the small-angle hypothesis. This indicates that much higher values of the surface anchoring energy, $\Delta\sigma \gg \sigma$, are needed for the curvature wall to completely disappear from the centers of the OS ($\Omega=\pi/2$). Figures 8(b) and 8(c) show, respectively, the equilibrium surface energy $\mu(x,\Omega)$ and period $P(x)$ as a function of x. The energy μ increases as the thickness h decreases, whereas P decreases. Figure 8(d) shows the optical path difference φ at the location of the curvature wall, where the thickness is $t=h\cos\Omega\approx h$ [Fig. 1(b)], as a function of h. To calculate φ, we used Eq. (1) with a tilt angle $\psi(z)=a\sin(z/h)$ for the splay-bend director profile at the curvature wall. We notice that φ monotonically increases with h and that the increase becomes almost linear at large values of h. In our experiments (Fig. 6, solid line), we used these properties to indirectly determine h from measured values of φ.

So far we have calculated the difference in surface energies μ [Eq. (10)] between an array of OSs and a reference uniform texture, that was chosen to be homeotropic. However, the results are valid also for a planar reference texture, with layers normal to the surface. In this case, $\Delta\sigma=\sigma_p'-\sigma_h'>0$ is the difference in surface energies between the planar (σ_p') and homeotropic (σ_h') alignment at the Sm*A*-air interface. Therefore, as the thickness h decreases, OSs disappear at the critical thickness h_0 given by Eqs. (7) and (8), where $\Delta\sigma$ is the surface energy required to reorient the LC molecules by 90° at the interface with the *weakest* anchoring. For $h<h_0$ the texture becomes uniform across the film thickness and oriented along the direction of the strongest anchoring.

V. DISCUSSION

One of the main advantages of using mica to study arrays of OSs is that the planar anchoring of 8CB on mica is monostable in each cleavage domain where the surface lattice is uniform [20,22]. By carefully cleaving mica plates, one can obtain large cleavage planes of area up to 1 cm^2 (see typical application for the surface force apparatus in Refs. [22,31]). Therefore, 8CB on mica creates uniform periodic arrays of straight OSs of much larger extent than previously obtained on multistable MoS_2 surfaces [13,23]. Moreover, mica is transparent to visible light, which is an advantage for application in photonics compared to opaque substrates [13].

These features helped us establish the geometry of the OS in the arrays, presented in Figs. 1(b) and 1(d), with respect to the film thickness and the local direction of planar anchoring on mica. The most significant validation of our model is given in Fig. 6, where the measured values of the period p of the array and of the optical path difference φ at the curvature wall are compared to a theoretical curve obtained for well-known values of Σ [29,30], λ [25], and the refractive indices n_e and n_o of 8CB [32] and for small core energies [$\alpha\approx 10$ in Eq. (7)]. The only adjustable parameter was the surface energy $\Delta\sigma$ required to reorient the molecules by 90° at the surface with weakest anchoring. $\Delta\sigma$ is analogous to the *zenithal* (out-of-plane) strength of the anchoring for a nematic with a surface energy obeying the Rapini-Papoular law: $\sigma(\psi)=\sigma_0+\Delta\sigma\sin^2\psi$, where ψ is the tilt angle and σ_0 is a constant [20].

A value of $\Delta\sigma=\sigma/2$ was chosen so as to cover the entire range of periods over which ordered arrays could be resolved by optical microscopy, from the transition to the FCD lattice at $p_{max}\approx 4.2$ μm down to $p_{min}\approx 0.5-0.6$ μm. The model correctly reproduces the magnitude of p and φ, and the slope of the $\varphi(p)$ curve. The theoretical line is slightly shifted from the experimental points to higher values of φ, most likely because the theoretical value of φ was calculated at the exact location of the wall, whereas φ was measured over a finite area of lower birefringence surrounding the curvature wall. The value of $\alpha\approx 10$ used for Eq. (7) has been calculated using core energy $F_{core}\approx K$ and radius $r_c\approx\lambda$ [6,17,26]. If we consider higher values of $F_{core}/K\approx c\approx 50$ and $r_c\approx 50\lambda$, recently found for OSs of 8CB on MoS_2 [27], we obtain $\alpha\approx c\approx 50$. In this case, one has to consider a higher anchoring energy, $\Delta\sigma\approx\sigma/1.3$, to reproduce the experimental $\varphi(p)$ curve down to the minimum period p_{min}, while the slope of the $\varphi(p)$ curve is only slightly increased (not shown). This shows that our analysis cannot precisely determine F_{core} and r_c. In fact, an increase of the core radius and energy of a disclination reduces by a comparable amount the volume and elastic energy of the layers wrapped around the disclination. As a result, only slight adjustments of the anchoring energy $\Delta\sigma$ are required to account for large changes of F_{core} and r_c.

Our model appears to correctly describe the defect domain structure as that of an OS, characterized by the presence of curvature walls and curved cylindrical layers, which have also been observed on MoS_2. In particular, the expression for the dilation energy of curvature walls [Eq. (5)] appears to be correct. Such agreement between experiment and theory could not be obtained for MoS_2, where 8CB form stripes of uniform homeotropic alignment alternating with streaks—a feature that could not be accounted for in theoretical models [13].

From the period of the linear arrays measured on mica in the range $[p_{min},p_{max}]$ we calculated the range of thicknesses

$[h_{min}, h_{max}]=0.8-17$ μm (Fig. 6) where OSs could be resolved. At a certain critical thickness h_0, OSs should become energetically unfavorable and disappear to the advantage of a uniform texture. Our measurements showed that the OS texture at the edge of the droplet continued into a birefringent (non homeotropic) texture without any evident structural transition. This could be an indication that the uniform texture was planar or that OSs are still present at small thicknesses, but no more resolved by optical microscopy. Preliminary measurements with an atomic force microscope proved to be difficult in this region, possibly because small streaks create an undulation of the 8CB/air interface that is too shallow to be observed in noncontact mode [13].

As a result, our measurements provide an upper value for the critical thickness, $h_0 \leqslant h_{min}=0.8$ μm and lower bound, $\Delta\sigma \geqslant 15$ mJ/m^2, for the strength of the *smectic* zenithal anchoring. We stress that this value of $\Delta\sigma$ refers to both interfaces: the homeotropic 8CB/air interface as well as the planar 8CB/mica interface. If one of the two anchorings was weaker than 15 mJ/m^2, a uniform texture aligned along the direction of the strongest anchoring would appear for some thickness $h > h_{min}$.

The value of $\Delta\sigma$ is much higher than the typical anchoring strength of a *nematic* LC [20,33]: $\Delta\sigma < 1$ mJ/m^2. In the Sm*A* phase, deviations of the surface director from the anchoring direction require compression or dilation of the layers, eventually leading to the creation of structural defects near the surface [34]. It has been calculated [35] that the energy per unit area required for large deviations is of the order of $K/\lambda \approx 10$ mJ/m^2, which is close to the value of $\Delta\sigma$ found in our experiments. However, an explanation based on general properties of the Sm*A* phase cannot account for the fact that OSs of the type of Fig. 1(d) have been observed so far only for mica and MoS_2. There must be a specific interaction between 8CB molecules and these substrates that produces a high value of $\Delta\sigma$ and stabilizes the OS structure. Most likely, this is related to the extreme smoothness of such substrates (rms roughness ~ 1 Å) and to the presence of a highly ordered, lattice-type monolayer of LC molecules adsorbed on the surface [23]. Indeed, the anchoring appears to be very strong already in the nematic phase of 8CB on MoS_2 [36] and for other nematic nCB compounds on mica [31,37].

OSs are usually observed in Sm*A* samples under symmetric homeotropic anchoring conditions, where they appear as curved, winding domains with a typical transverse striation [15–17,38]. Striation can be due to an intrinsic instability of straight curvature walls [39], which tend to slightly undulate along the main streak axis [15] or to the presence of a periodic sequence of FCDs oriented with the minor axis of the ellipse along the streak [16]. In both cases, the horizontal orientation of the director (in a plane containing both disclinations *c* of Fig. 1(b)) varies along the streak. On the contrary, straight OSs have been observed only on mica and MoS_2, where they are free of striation for small thicknesses. This indicates that the *azimuthal* (in-plane) strength of the planar anchoring is particularly high compared to other substrates: horizontal deviations from the easy axis are highly restrained. Indeed, the presence of a highly-ordered monolayer lattice of LC molecules adsorbed on a crystalline surface [40] produces well-defined macroscopic anchoring directions to the LC [23]. One expects such surfaces to provide a more directional planar anchoring than amorphous surfaces such as rubbed glass, resulting in a higher azimuthal strength.

Limited azimuthal deviations of the director from the easy axis appear on mica in isolated striated streaks and FCD (Fig. 7) for large thickness only. The maximum azimuthal deviation occurs in the fragmented FCD and is the half-aperture $\pi/2 \approx 37°$ [Fig. 7(c)] of the fan-shaped texture. To our knowledge, this type of FCD lattice has been observed only once [10,19] for a thermotropic LC confined between solid plates under hybrid anchoring conditions. Describing the geometry of fragmented FCDs in free Sm*A* films and deriving the relation between their energy and size is beyond the scope of this article. It is clear however that thickness is the main parameter for the appearance of these structures. Theory is available only for lattices of toroidal FCDs formed on surfaces that induce degenerate planar anchoring [6–8,12]. In this case, the azimuthal anchoring strength is zero and no other birefringent structure is observed as the thickness changes.

VI. CONCLUSIONS

We have shown that it is possible to obtain large arrays of remarkably straight, parallel and periodic OSs in thin films of Sm*A* deposited on mica in air. This is due to a particularly high strength of both zenithal and azimuthal anchoring on crystalline substrates. Comparing measurement of optical birefringence with a simple theoretical model, we were able to describe the variation of the array period as a function of the film thickness. The system also shows a thickness-induced transition from 1D arrays to a more complex geometry of fan-shaped, fragmented focal conic domains arranged in 2D lattices. The possibility of preparing patterns of size and dimensionality depending on the thickness could be used for guided spatial organization and alignment of nanoparticles of different size and shapes (spheres, rods, disks) in Sm*A*-nanoparticle mixtures.

ACKNOWLEDGMENTS

We are grateful to Professor Philippe Barois of the CRPP-CNRS of Bordeaux for fruitful discussions on the theoretical model. We thank Professor R. Barberi and Professor Bartolino for their support and comments on the manuscript.

[1] K. Busch and S. John, Phys. Rev. Lett. **83**, 967 (1999).
[2] V. I. Kopp, Z. Q. Zhang, and A. Z. Genack, Prog. Quantum Electron. **27**, 369 (2003).
[3] X. Wang, D. H. Kwon, D. H. Werner, I. C. Khoo, A. V. Kildishev, and V. M. Shalaev, Appl. Phys. Lett. **91**, 143122 (2007).
[4] D. K. Yoon, M. C. Choi, Y. H. Kim, M. W. Kim, O. D. Lavrentovich, and H. T. Jung, Nature Mater. **6**, 866 (2007).
[5] G. Friedel, Ann. Phys. (Paris) **18**, 273 (1922).
[6] J. B. Fournier, I. Dozov, and G. Durand, Phys. Rev. A **41**, 2252 (1990).
[7] M. C. Choi, T. Pfohl, Z. Y. Wen, Y. L. Li, M. W. Kim, J. N. Israelachvili, and C. R. Safinya, Proc. Natl. Acad. Sci. U.S.A. **101**, 17340 (2004).
[8] V. Designolle, S. Herminghaus, T. Pfohl, and C. Bahr, Langmuir **22**, 363 (2006).
[9] C. Blanc and M. Kleman, Eur. Phys. J. B **10**, 53 (1999).
[10] L. Z. Ruan, J. R. Sambles, and I. W. Stewart, Phys. Rev. Lett. **91**, 033901 (2003).
[11] P. G. De Gennes and J. Prost, *The Physics of Liquid Crystals* (Oxford University Press, Oxford, 1974).
[12] C. Blanc and M. Kleman, Phys. Rev. E **62**, 6739 (2000).
[13] J.-P. Michel, E. Lacaze, M. Alba, M. de Boissieu, M. Gailhanou, and M. Goldmann, Phys. Rev. E **70**, 011709 (2004).
[14] M. Kléman, *Points, Lines and Walls in Liquid Crystals, Magnetic Systems and Various Ordered Systems* (Wiley, New York, 1983).
[15] M. B. Schneider and W. W. Webb, J. Phys. (Paris) **45**, 273 (1984).
[16] P. Boltenhagen, O. D. Lavrentovich, and M. Kléman, J. Phys. II **1**, 1233 (1991).
[17] Z. Li and O. D. Lavrentovich, Phys. Rev. Lett. **73**, 280 (1994).
[18] D. Dash and X. L. Wu, Phys. Rev. Lett. **79**, 1483 (1997).
[19] O. D. Lavrentovich and M. Kleman, Phys. Rev. Lett. **97**, 159801 (2006).
[20] B. Jerome, Rep. Prog. Phys. **54**, 391 (1991).
[21] N. Matsuhashi, Y. Okumoto, M. Kimura, and T. Akahane, Jpn. J. Appl. Phys., Part 1 **41**, 4615 (2002).
[22] S. H. J. Idziak, C. R. Safinya, R. S. Hill, K. E. Kraiser, M. Ruths, H. E. Warriner, S. Steinberg, K. S. Liang, and J. N. Israelachvili, Science **264**, 1915 (1994).
[23] E. Lacaze, J. P. Michel, M. Goldmann, M. Gailhanou, M. De Boissieu, and M. Alba, Phys. Rev. E **69**, 041705 (2004).
[24] M. J. Bradshaw and E. P. Raynes, J. Phys. (Paris) **46**, 1513 (1985).
[25] M. Benzekri, T. Claverie, J. P. Marcerou, and J. C. Rouillon, Phys. Rev. Lett. **68**, 2480 (1992).
[26] M. Kleman and O. D. Lavrentovich, Eur. Phys. J. E **2**, 47 (2000).
[27] J.-P. Michel, E. Lacaze, M. Goldmann, M. Gailhanou, M. de Boissieu, and M. Alba, Phys. Rev. Lett. **96**, 027803 (2006).
[28] For negative β one can only have a positive minimum.
[29] M. Tintaru, R. Moldovan, T. Beica, and S. Frunza, Liq. Cryst. **28**, 793 (2001).
[30] H. Schuring, C. Thieme, and R. Stannarius, Liq. Cryst. **28**, 241 (2001).
[31] B. Zappone, Ph. Richetti, R. Barberi, R. Bartolino, and H. T. Nguyen, Phys. Rev. E **71**, 041703 (2005).
[32] S. J. Elston and J. R. Sambles, *The Optics of Thermotropic Liquid Crystals* (CRC, New York, 1998).
[33] L. M. Blinov and V. G. Chigrinov, *Electrooptic Effects in Liquid Crystal Materials* (Springer-Verlag, Berlin, 1996).
[34] C. E. Williams and M. Kléman, J. Phys. Colloq. **3**, 315 (1975).
[35] G. Durand, Liq. Cryst. **14**, 159 (1993).
[36] E. Lacaze, J.-P. Michel, M. Alba, and M. Goldmann, Phys. Rev. E **76**, 041702 (2007).
[37] L. M. Blinov and A. A. Sonin, Mol. Cryst. Liq. Cryst. **179**, 13 (1990).
[38] S. A. Asher and P. S. Pershan, Biophys. J. **27**, 393 (1979).
[39] R. Bidaux, N. Boccara, G. Sarma, and L. De Seze, J. Phys. (Paris) **34**, 661 (1973).
[40] E. Lacaze, P. Barois, and R. Lacaze, J. Phys. I **7**, 1645 (1997).